RSC Advances

PAPER

View Article Online
View Journal | View Issue

Cite this: *RSC Adv.*, 2020, **10**, 20395

Low temperature conversion of levulinic acid into γ-valerolactone using Zn to generate hydrogen from water and nickel catalysts supported on sepiolite†

Adrián García,[a] Rut Sanchis,[a] Pablo J. Miguel,[a] Ana M. Dejoz,[a] María Pilar Pico,[b] María Luisa López,[c] Inmaculada Álvarez-Serrano,[c] Tomás García[d] and Benjamín Solsona*[a]

Received 8th April 2020
Accepted 21st May 2020

DOI: 10.1039/d0ra04018e

rsc.li/rsc-advances

In the present article, γ-valerolactone has been obtained from levulinic acid with a yield exceeding 25% using very mild conditions without feeding hydrogen (30 °C, atmospheric pressure, water as the hydrogen source). The overall reaction conducted is a two-step process: first, a redox reaction involving the oxidation of metallic Zn to ZnO for *in situ* hydrogen production through the water splitting reaction and, second, a catalytic reaction involving Ni-supported catalysts for the production of γ-valerolactone from levulinic acid. Ni active sites have been supported on sepiolite, an abundant and cheap material. The nickel particle size has been demonstrated to be a parameter of paramount importance determining the catalytic activity, since the best catalytic performance is obtained with the smallest Ni nanoparticles. This combination of Zn and Ni supported on sepiolite shows a good catalytic stability after three catalytic runs.

Introduction

In an extensive study carried out by the US Department of Energy,[1] 12 compounds from sugars were identified as easily removable and with extraordinary transformation potential into high value compounds. One of these compounds is levulinic acid. As is widely known, biomass can be a sustainable source for the production of fuels as an alternative to petroleum derivatives.[2–5] Interestingly, levulinic acid (LA) can be transformed into γ-valerolactone (GVL),[6–8] which is a compound with high interest as a possible substitute for petroleum fuels, since it can be easily transformed into high-energy density fuels. Another of the great advantages of γ-valerolactone is its very low toxicity. Therefore, it is considered an ideal liquid fuel (or fuel precursor) to be transported and stored.[9,10]

The selective conversion of LA into GVL can take place by homogeneous and/or heterogeneous catalysis.[11] Typical catalysts are based on noble metals, since these materials achieve the highest productivity to GVL.[12–16] Among the catalysts based on noble metals, ruthenium yields the best results. However, as noble metals are expensive, different options involving cheaper materials have been proposed. Fortunately, supported catalysts of either non-noble metals[17] or mixed metal oxides,[18,19] if properly optimized, have proven to be almost as efficient as catalysts based on noble metals. Nickel is one of the most efficient non-noble metals used in the conversion of LA into GVL.[20–25]

In the last decades, different metals have been supported on low-cost minerals and tested in this or in similar catalytic reactions. One of these materials is sepiolite, which has been used as a catalytic support in many reactions.[26–28] Sepiolite is a hydrous magnesium silicate which presents many applications. Its main use is as absorbent, although it presents some other utilities such as pharmaceutical products, detergents, phytosanitary carriers, animal food…[29] Sepiolite presents important advantages over most of the conventional catalytic supports. Firstly, it is extremely cheap as it can be directly obtained from sepiolite quarries. Second, sepiolite is a fibrous clay containing ribbons that presents microcavities in a fibrous structure which can be important in catalysis. Accordingly, Guerrero-Torres *et al.* studied the incorporation of Ni active sites on sepiolite support by different preparation methods and these catalysts were assessed in the hydrogenation of furfural.[30] As expected, it was found that the dispersion and size of the Ni metal particles was depending on the preparation method, modifying the interaction between metal particles and sepiolite support. Ni supported on sepiolite, if properly synthesized,

[a]*Departament d'Enginyeria Química, ETSE, Universitat de València, Av. Universitat, 46100 Burjassot, Valencia, Spain. E-mail: benjamin.solsona@uv.es*

[b]*Sepiolsa, Avda. del Acero, 14-16, Pol. UP-1 (Miralcampo), 19200 Azuqueca de Henares, Spain*

[c]*Departamento de Química Inorgánica, Facultad de Ciencias Químicas, Universidad Complutense de Madrid, 28040 Madrid, Spain*

[d]*Instituto de Carboquímica (CSIC), C/Miguel Luesma Castán, 50018 Zaragoza, Spain*

† Electronic supplementary information (ESI) available. See DOI: 10.1039/d0ra04018e

achieved high performance for the decarbonylation of furfural to furan, being favored when small Ni nanocrystals were synthetized.

The conversion of LA into GVL presents some similarities with the furfural hydrogenation as both involve a hydrogenation step. However, an additional dehydration step is required for GVL production. In any case, these reactions necessarily require a hydrogen source. Different solutions are proposed in the literature, being most of the studies performed with high pressure H_2 in batch reactors, although feeding of high-pressure H_2 in continuous gas-phase systems has also been reported.[31] However, the storage and handling of high-pressure hydrogen involves a series of hazards due to its high flammability and low energy ignition. For these reasons, several alternatives have been studied in order to generate *in situ* hydrogen, avoiding the use of molecular H_2. One of these solutions is the use of formic acid as a hydrogen donor. Formic acid can be obtained from sugar transformation together with levulinic acid. Then, depending on the process conditions, formic acid decomposes to give CO and H_2 and this H_2 can be later used for the hydrogenation of LA to GVL[32–36] avoiding the supply of external hydrogen. Unfortunately, harsh reaction conditions are usually required.

The LA to GVL transformation can also take place without the addition of molecular hydrogen by catalytic transfer hydrogenation employing different types of alcohols as hydrogen donors, such as 2-propanol, 2-butanol or isopropyl alcohol.[37–40] Then, catalytic transfer hydrogenation *via* the Meerwein–Ponndorf–Verley presents, selecting the reaction conditions, good chemo-selectivity for the carbonyl groups reduction and this allows this reaction can take place with reasonably high efficiency.

Another interesting and simple option to obtain *in situ* H_2 is the addition of a certain amount of a suitable metal to the reaction media containing water (for example, alkaline and alkaline-earth metals or some transition elements). Then, H_2 production is accomplished through a redox reaction involving metal oxidation and water splitting reaction, $Me + H_2O \rightarrow MeO + H_2$ (or $Me + H_2O \rightarrow MeOH + \frac{1}{2}H_2$).[21,41] This reaction, which is thermodynamically favored, can even take place at room temperature. It must be indicated that the metal added to water does not act as a catalyst in obtaining hydrogen but simply as a reagent. Therefore, the amount of hydrogen produced will depend on the amount of metal used.

H_2 production from the redox reaction of metal and water is not a new concept.[41–43] In fact, metal–water reactions have been proposed to be used for fuel cell devices in portable applications, such as computers and vehicles. Unfortunately, these applications do not seem to be economically profitable because of the large amount of metals required for hydrogen production. Positively, aluminum–water interaction for H_2 production has shown to be reasonably interesting for some specific non-portable applications, such as electronic devices.[43] Herein, we have proposed the formation of *in situ* hydrogen for its use in hydrogenation processes, preventing the inconveniences arising from the direct use of high-pressure molecular hydrogen. Specifically, we have selected Zn among the different

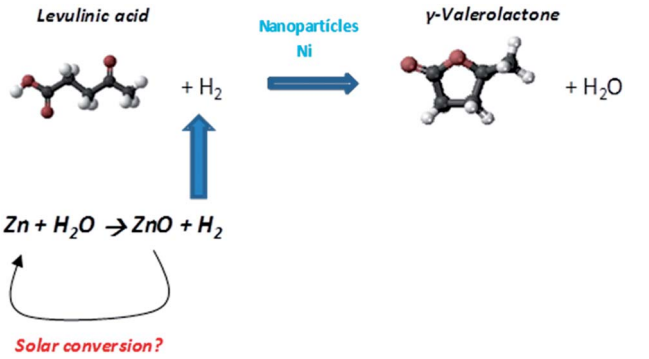

Scheme 1 Scheme showing the transformation of levulinic acid into γ-valerolactone using Ni catalysts and Zn.

metals that in the presence of water could lead to the formation of H_2, because its evolution is a non-violent reaction, in contrast with the use of some alkali metals such as potassium or sodium. In the Zn–water reaction media, H_2 generation is carried out according to the following reaction:

$$Zn + H_2O \rightarrow ZnO + H_2;\ \Delta H = -63\ \text{kJ mol}^{-1}\ (298\ \text{K}) \quad (1)$$

From a green chemistry point of view, the main problem associated with the use of Zn as reactant could be the fact that after reaction (1) Zn is almost completely oxidized to ZnO. Hence, a reduction regeneration step needs to be carried out for its use in a cyclic operation. An interesting green solution would be the use of solar chemical reactors where Zn yields from ZnO greater than 90% has been reported.[44] Thus, a cyclic operation could be proposed where, firstly, the hydrogenation of levulinic acid to gamma-valerolactone is carried out with *in situ* H_2 generated throughout the Zn-water redox system and, secondly, Zn is regenerated from ZnO using solar energy. To our knowledge, although this zinc reuse strategy would not sort out the energy problem of the global process, it could be an interesting green alternative that deserves to be studied.

The transformation of LA into GVL at low temperatures has been scarcely reported and always with direct supply of hydrogen.[45,46] In the present article, we have newly proposed a green alternative involving the use of Zn to obtain hydrogen from water and non-noble metal catalysts based on Ni (Scheme 1) in order to transform LA into GVL. Reaction conditions were very mild using reaction temperatures close to room temperature, atmospheric pressure and aqueous media. Therefore, the main novelty of this article lies in the use of low temperature and the absence of pressurized molecular hydrogen in the catalytic conversion of levulinic acid into γ-valerolactone. Moreover, the active sites of the catalysts employed are not noble metals and the support used is sepiolite, an abundant, cheap and natural clay.

Results and discussion

Initially, commercial Zn was tested at very mild conditions: 30 °C, atmospheric pressure and levulinic acid solution in

Table 1 Physico-chemical characteristics of the Ni/sepiolite catalysts synthesized

Catalyst	Preparation method	Ni wt%	S_{BET} ($m^2\ g^{-1}$)	V^a ($cm^3\ g^{-1}$)	D_p (Å) ($4V/A$)^b
Sepiolite	Support	0	242	0.392	98.9
1Ni/sep-ox	Oxalic acid in ethanol	1	202	Not determined	Not determined
2Ni/sep-ox	Oxalic acid in ethanol	2	202	0.447	118.3
5Ni/sep-ox	Oxalic acid in ethanol	5	210	Not determined	Not determined
10Ni/sep-ox	Oxalic acid in ethanol	10	218	0.480	120.6
100Ni-ox	Oxalic acid in ethanol	100	7	—	—
2Ni/sep	Simple impregnation	2	204	Not determined	Not determined

[a] Single point adsorption total pore volume at $p/p^0 = 0.99$. [b] Desorption average pore width.

water. Transformation of LA into GVL was observed although with very low conversion. Interestingly, the GC analysis of the gas evolved showed hydrogen formation. Subsequently, pure bulk metallic nickel catalyst (commercial) was tested in the same experimental conditions. Again, the transformation of levulinic acid was marginal, being the formation of valerolactone negligible. Moreover, gas analysis did not show any hydrogen formation. Then, Zn and metallic nickel were simultaneously incorporated to the reaction media. Interestingly, some GVL conversion was observed, being higher than that theoretically obtained from the sum of the experiments with Zn and Ni, separately. Therefore, it could be assumed that this reaction system could produce GVL from LA at mild conditions. However, catalyst optimization would be needed since the number of available Ni sites in bulk catalysts was rather limited. Accordingly, Ni nanoparticles were finely dispersed in a low-cost support by different preparation methods.

As support we selected sepiolite, a natural but complex material with formula $Mg_4Si_6O_{15}(OH)_2 \cdot 6H_2O$. High availability, low cost and relatively high surface area, which allows a proper dispersion of metals on its surface, are the main advantages of this support. The most relevant compositional and structural characteristics of the provided sepiolite were obtained from previous XRD, TGA, ^{29}Si-NMR, SEM and EDS data.[47] Thus, sepiolite showed an orthorhombic structure with cell parameters $a = 13.400$, $b = 26.964$ and $c = 5.2626$ Å, and did not present any secondary phase or impurities. Besides, this support had a surface area of 250 $m^2\ g^{-1}$, which was slightly decreased after reduction (242 $m^2\ g^{-1}$).

Different amounts of nickel (1, 2, 5 and 10 wt%) were supported on the sepiolite support (Table 1) by a wet impregnation method using oxalic acid (Ni/sep-ox series). Oxalic acid was added since, as reported, it favors the creation of small Ni nanoparticles finely dispersed on the support. Again, marginal GVL formation was observed for these materials and the analysis of the gas did not show any hydrogen formation.

Then, Zn and Ni/sep-ox catalysts were simultaneously tested for LA hydrogenation. Interestingly, a notorious transformation of levulinic acid was always observed, being the selectivity to GVL higher than 96%. The GC-MS analysis mainly detected GVL as the reaction product (see ESI, Fig. S1†), although traces of other compounds were also identified (see ESI, Fig. S2†). Table 2 shows the influence of the nickel content on the yield to GVL as well as on the productivity per Ni site. Interestingly, the maximum yield was achieved at Ni-contents between 2 and 5 wt%, whilst the highest productivity per Ni site was attained by those catalysts with the lowest Ni-loading (1 and 2 wt% Ni). It is worth commenting that catalytic activity was clearly related to the synergetic effect between the Ni supported catalysts and the Zn–water redox system since the sum of the GVL yields obtained in individual control experiments using Zn and Ni/sepiolite hardly reached 2%. Additionally, a control reaction using the bare sepiolite support with Zn showed a comparable GVL yield to the Zn control reaction, proving the inert role of sepiolite in the reaction. Remarkably, the use of both Zn and Ni/sepiolite led to conversions higher than 25% for Ni loadings of 2 and 5 wt%. These excellent results can be linked to the presence of a cascade-type reaction where, first, the *in situ* H_2 generation throughout the redox Zn–water system and, second, the catalytic hydrogenation/dehydration of LA to GVL over metallic Ni sites, are produced. The use of oxalic acid in the preparation procedure was demonstrated to be beneficial for the production of GVL. Then, the catalyst prepared in the absence of oxalic acid 2Ni/sep obtained GVL yield *ca.* 1/3 of that obtained by the analogue catalyst prepared with oxalic acid (Table 2).

The influence of the reaction temperature was studied for low temperatures (in the 30 to 50 °C range) on the 2Ni/sep-ox + Zn combination. An increase of the temperature involves a faster reaction between Zn and water and, also, for the LA to GVL transformation. Then, the amount of available hydrogen in the media could vary in each experiment and then the effect of the temperature on the overall reaction could be uncertain. However, the trend observed is an increase in the GVL formation with the reaction temperature, as it could be expected. Then, at 30 °C the GVL yield was 26.9%, at 40 °C 34.7% and at 50 °C 40.5%.

The possible leaching of nickel in the Ni/sepiolite catalysts under reaction conditions was also studied. For that, after a standard experiment with 2Ni/sep-ox + Zn (GVL yield = 26.1%), the solids were removed by filtration and the liquid with the GVL obtained in the previous experiment was collected. Then, this liquid together with fresh Zn was left for two more hours in typical reaction conditions. The analysis of the solution showed a GVL yield of 28.7%. This result fitted with the expected slight increase in the GVL due to the addition of fresh

Table 2 Catalytic performance of Ni and sepiolite catalysts with the assistance or not of Zn[a]

Catalyst	LA conversion (mol%)	Yield to GVL[b] (mol%)	GVL productivity[c]	GVL productivity per Ni[d]
Zn	2.1	1.98	0.07	—
Ni	<1	Traces	—	—
Zn + Ni	3.5	3.5	0.12	0.12
Sep	0	0	0	—
2Ni/sep-ox	<1	Traces	—	—
Zn + sep	2.1	2.1	0.08	—
Zn + 1Ni/sep-ox	17.5	17.0	0.59	60.0
Zn + 2Ni/sep-ox	26.9	26.1	0.91	46.0
Zn + 5Ni/sep-ox	26.1	25.3	0.88	17.9
Zn + 10Ni/sep-ox	18.2	17.8	0.62	6.3
Zn + 100Ni-ox	7.0	6.5	0.23	0.23
Zn + 2Ni/sep	10.0	9.6	0.33	16.9

[a] Reaction conditions in text. Standard conditions. 2 h experiment. [b] Yield to GVL. The selectivity to GVL exceeds 95% in all cases. [c] Per mass of Ni-catalyst as mol_{GVL} $(kg_{cat}\ h)^{-1}$. [d] Per mass of Ni in the Ni-catalyst as mol_{GVL} $(kg_{Ni}\ h)^{-1}$.

Zn. Then, it could be concluded that either there was no nickel leaching or dissolved nickel did not produce GVL.

Ni/sepiolite catalysts were characterized by several techniques in order to see the reason for the different reactivity of Ni/sepiolite catalysts. N_2 adsorption isotherms pointed out that the support and all the catalysts exhibited a type IV isotherm, related to mesoporous materials (Fig. 1). Hysteresis cycles due to capillary condensation phenomena were clearly observed in all catalysts. The obtained pore distribution curve for the sepiolite (Fig. 1C) showed that the average pore diameter was around 4 nm, which was coherent with previously reported data for this type of clay.[48,49] No appreciable differences were observed in the profile of the support and the supported nickel catalysts. Regarding to the pore distribution of the Ni supported catalysts (Fig. 1C), maxima at *ca.* 3.9 nm were observed in all the Ni/sepiolite samples, suggesting that nickel was not blocking the sepiolite pores. The addition of nickel led to a slight drop in the surface area for the catalysts compared to the pure support. The surface area of the support was 242 $m^2\ g^{-1}$ whereas that of the supported nickel was between 202 and 218 $m^2\ g^{-1}$. Finally, the sepiolite free Ni catalyst had a low surface area of only 7 $m^2\ g^{-1}$, being this value close to that obtained by others authors in bulk Ni catalysts.[48,49]

Fig. 2 shows XRD patterns of the Ni-based catalysts and their NiO precursors before and after the reduction step. As can be observed in Fig. 2A, the NiO/sepiolite precursors presented the diffraction peaks typical of sepiolite. Interestingly, the thermal treatment did not modify the initial sepiolite structure. Thus, the only loss of water corresponded to zeolitic water, *i.e.* there was not a folding of sepiolite after the reduction process. Moreover, wide reflections from cubic NiO (NiO, JCPDS: 47-1049) could be observed in all cases, suggesting the small size of NiO crystals. The intensity of these NiO peaks enhanced when the nickel loading increased. In Fig. 2B, the diffractograms of

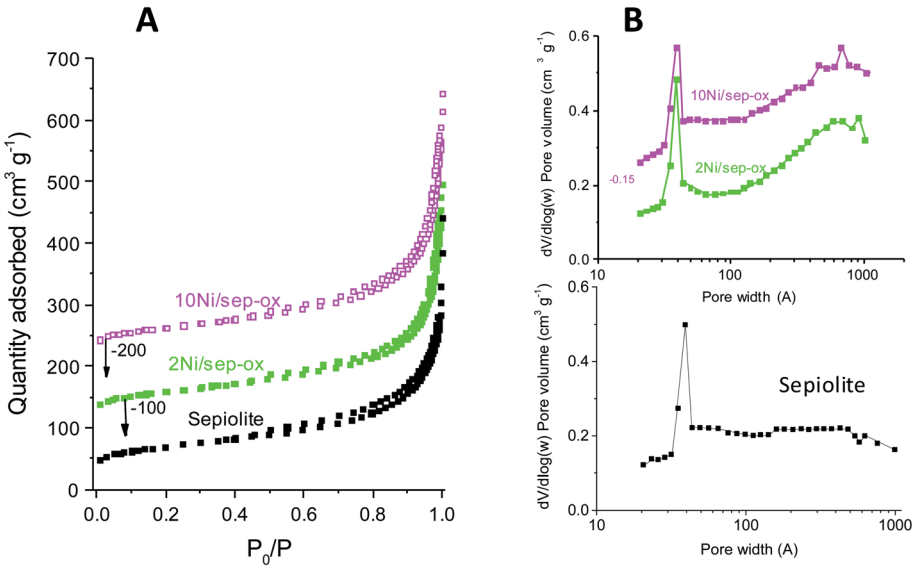

Fig. 1 N_2 isotherms patterns for sepiolite and Ni/sepiolite catalysts (A) and their corresponding pore distributions (B).

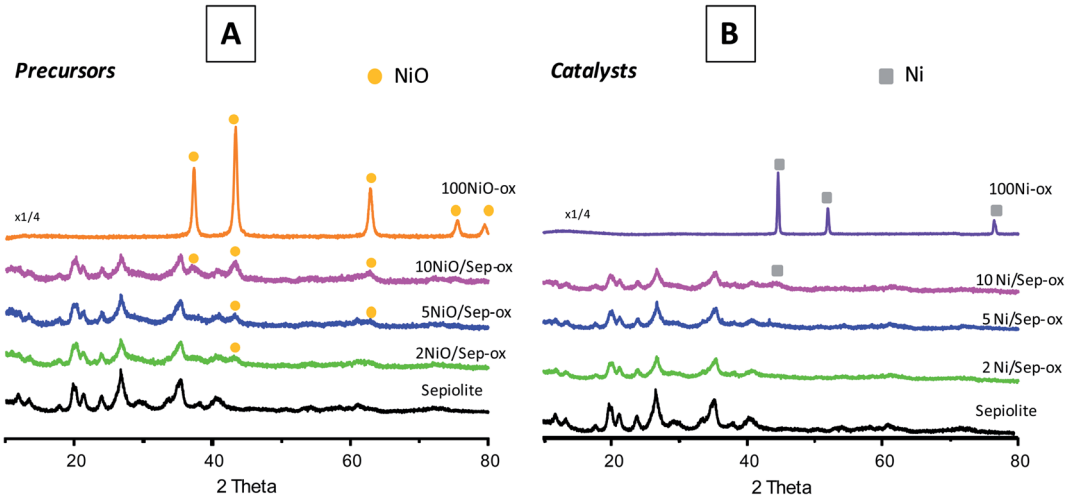

Fig. 2 XRD patterns of NiO/sepiolite precursors (A) and final reduced Ni/sepiolite catalysts (B) prepared by impregnation using ethanol.

the final reduced catalysts showed that nickel phase was only apparent in the catalysts with 10 wt% Ni, where a wide and low intensity peak at *ca.* 44° corresponding to metallic nickel (Ni, JCPDS: 01-1260) could be observed. This suggested that nickel was present in these catalysts in the form of very tiny particles. XRD peaks related to the support did not show any significant difference compared to pure sepiolite, pointing out that no important modification of the crystalline structure of the sepiolite support took place in Ni/sepiolite samples after the reduction step.

High resolution transmission electron microscopy (HRTEM) study was carried out to provide a more accurate view of the location and size of the Ni particles on the sepiolite support prepared with oxalic acid. Fig. 3 shows the HRTEM images of Ni catalysts with 2, 5 and 10 wt% Ni. Large rods of sepiolite support with variable size were apparent in these samples. The length of these rods largely varied from 50 nm to several μm whereas the width was in the 8 to 50 nm range. Nickel was in all cases detected as metallic nickel although some differences were observed among these catalysts. TEM images evidenced the crystallinity of the Ni nanoparticles, as indicated by the observed periodical contrasts of 0.20 nm in the images, which were assigned to (111) interplanar distances of cubic Ni (see inset of Fig. 3). Thus, they were well stabilized as metallic Ni, since they are not easily oxidized under air exposure, once supported on the sepiolite. Overall, using oxalic acid in the preparation method the obtained Ni nanoparticles were smaller in particle size compared to previously reported Ni–clay supported catalysts.[50,51] The catalyst with 2 wt% Ni presented zones of the support with low concentration of Ni particles and other areas with high concentration. This lack of uniformity could be due to the preparation method followed, as wet impregnation methods often lead to heterogeneous distributions of nanoparticles. However, it must be noted that Ni nanoparticles were

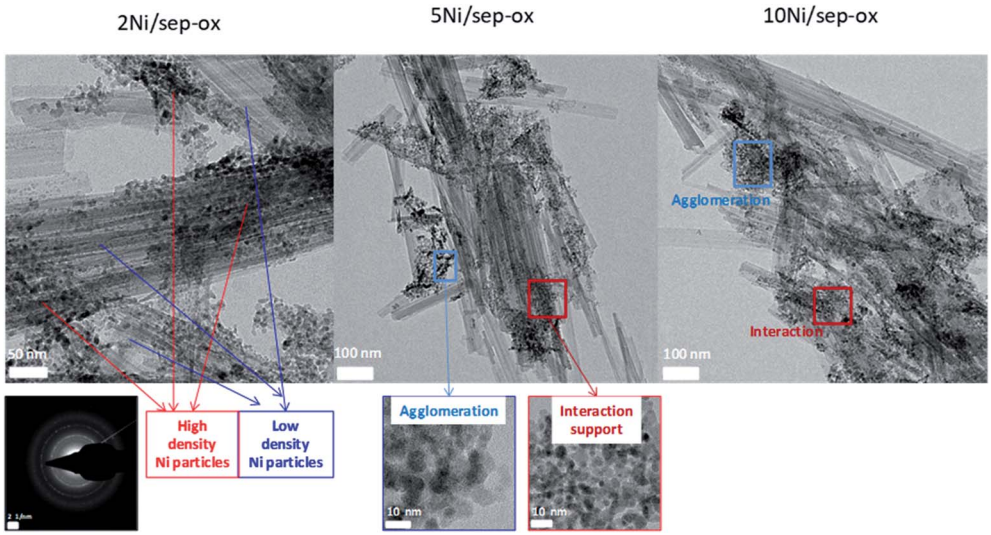

Fig. 3 TEM images of Ni/sepiolite catalysts prepared by wet impregnation method.

in all cases over the support either directly or in a few cases forming a couple of layers, probably due to their magnetic nature. As shown in Fig. 4, particle size distribution was quite homogeneous, presenting a small average size, *ca.* 3 nm, with 80% of the particles being smaller than 4 nm. Some agglomerations of free Ni particles were also apparent, leading to aggregates of 5–6 nm. In the catalyst with 5 wt% Ni, a higher amount of Ni nanoparticles was observed on the support surface. Additionally, more agglomerations of Ni nanoparticles were also visible. Finally, a higher density of nanoparticles was apparent in the 10 wt% Ni catalyst. In addition, a higher degree of agglomeration was attained although some isolated nanoparticles supported on sepiolite were also observed. Therefore, we can conclude from detailed microstructural analysis that the key parameters governing the catalytic performance of LA hydrogenation seem to be the size of the Ni nanoparticles and its dispersion, being preferred those small Ni nanoparticles finely dispersed on the whole external surface of the sepiolite fibers.

GVL was obtained from LA at very mild conditions (temperature close to room temperature (30 °C), atmospheric pressure and water solution) using Zn as non-catalytic *in situ* generator of hydrogen from water and supported Ni materials as active catalysts. This combination led to an excellent performance in terms of LA conversion and GVL selectivity. However, catalyst stability is another important parameter that needs to be studied. Re-use testing experiments were undertaken using 2Ni/sep-ox sample as catalyst and Zn (Fig. 5). After a standard reaction, the Ni catalyst and Zn were collected after washing with deionised water, filtering and drying at 120 °C. Not all the solid could be recovered as it remained in the filter paper and the reactor walls, so that a loss of weight of *ca.* 20% was observed. We assume that the loss of weight is equal for both Zn and the Ni-catalyst. This procedure was carried out for three times. This way, after 3 uses previous reduction, the GVL productivity observed decreased only *ca.* 20% compared to the productivity obtained with the fresh material.

To get deep into the role of Zn in the whole process, several experiments were carried out with Ni catalyst and adding different amounts of Zn, varying from 130 to 285 mg (Fig. S3†).

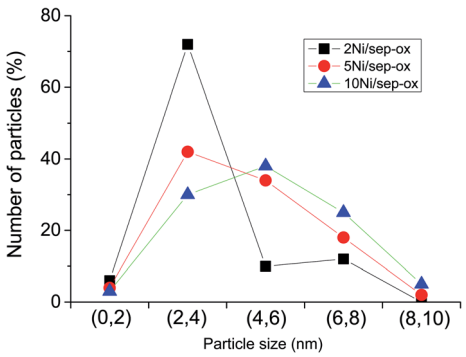

Fig. 4 Particle distribution showing the Ni particle size distribution of Ni/sepiolite catalysts prepared using oxalic acid. Symbols: (■) 2Ni/sep-ox, (●) 5Ni/sep-ox, (▲) 10Ni/sep-ox.

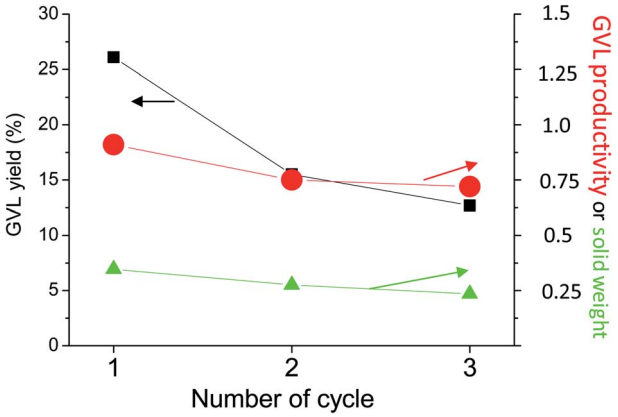

Fig. 5 Re-use testing of 2Ni/sep-ox and Zn at 30 °C. Symbols: GVL productivity in mol_{GVL} $(kg_{cat}\ h)^{-1}$ (●), yield to GVL (■), weight of solid loaded, Ni-catalyst plus Zn recovered, in g (▲). Remaining reaction conditions in Experimental section.

It was appreciated that the catalytic performance was maintained regardless of the excess amount of fresh Zn employed, probing that the amount of released hydrogen was not the rate limiting parameter in the LA hydrogenation.

For a standard experiment using 171.6 mg of Zn, 2.63×10^{-3} mol of H_2 would be produced in the case of a full Zn transformation into ZnO, according to reaction (1). On the other hand, the hydrogen released in a standard experiment with 2Ni/sep-ox and Zn was calculated. For this, the amount of hydrogen required for the transformation of LA into GVL, the amount of hydrogen released to the gas phase (which can be analyzed by GC and quantified knowing the free room of the flask) and the amount of hydrogen in the liquid phase (estimated by the Henry's law equation) were considered. Accordingly, a theoretical transformation of Zn into ZnO about 16% was determined, pointing out that a partial oxidation of Zn into ZnO is accomplished. In Fig. 6 we can see the TEM images of the 2Ni/sep-ox + Zn mixtures after use. Long sepiolite fibers with small nickel particles were found together with large Zn/ZnO particles of variable size (typically 50–100 nm wide and 100–500 nm long). The electron diffraction analyses showed that Zn was present as both metallic Zn and oxidized ZnO, in their respective hexagonal crystalline structures. The SAED results (Table S1†) cannot quantify accurately the content in Zn and ZnO but we observed some areas rich in Zn and others rich in ZnO. Therefore, these data corroborated the partial oxidation of Zn to ZnO during our experiment at standard conditions.

The separation of Ni/sepiolite catalysts and Zn could be possible by considering the different physical and magnetic properties of them but it would be easier if during the process Ni/sepiolite catalysts and Zn were not together. Moreover, we would like to highlight the paramount importance of *in situ* generated hydrogen. This issue was demonstrated in a final experiment using two interconnected three neck flasks where H_2 generation through the redox Zn–water reaction and LA hydrogenation were separately performed. Accordingly, metal Zn particles were suspended in a water solution under stirring

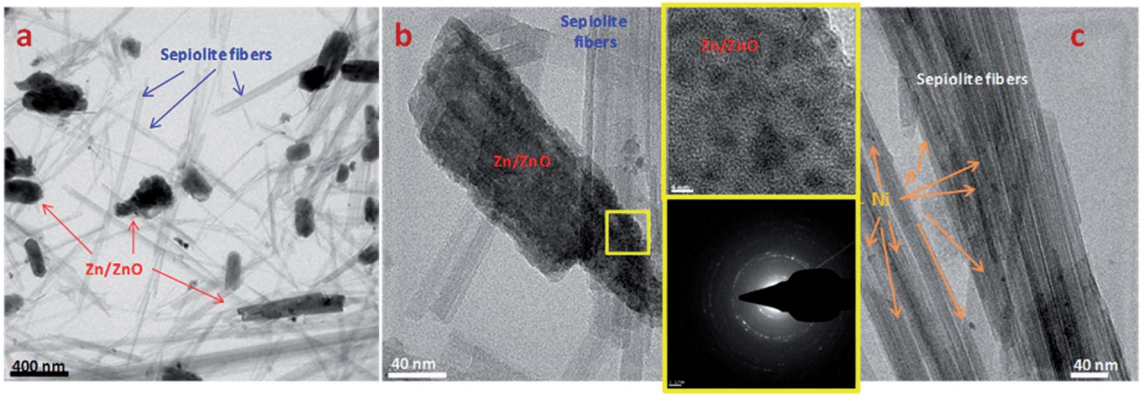

Fig. 6 TEM images of 2Ni/sep-ox + Zn after use at different magnifications. General view (a), image focused into a particle rich in Zn (b) and image focused into sepiolite fibers (c). The SAED pattern of (b) is included.

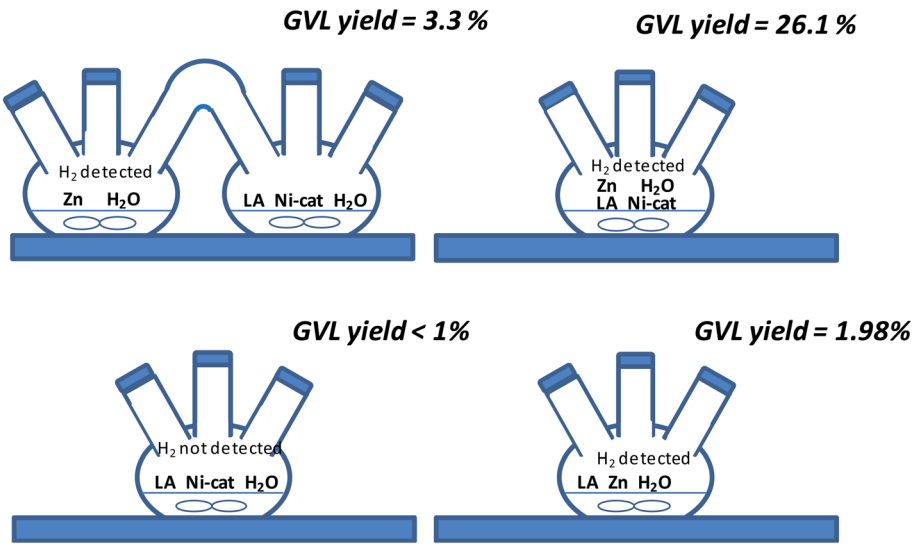

Fig. 7 Scheme of the different experiments conducted. Note: Ni-catalyst corresponds to 2Ni/sep-ox.

in the first flask, whilst a LA aqueous solution with Ni/sepiolite was set up in the second flask (see Fig. 7). The results obtained showed that although formation of GVL was possible, GVL yield (3.3%) was remarkably lower than that using the mixture Zn–Ni/sep-ox in a single flask (yield = 26.1%). Probably, atmospheric pressure hydrogen in the gas phase generated in one of the interconnected flasks only allowed a small amount of hydrogen dissolved into the water/LA/Ni/sepiolite mixture then preventing the hydrogenation of LA into GVL.

The relative reaction rate between the *in situ* generated hydrogen and the capacity of Ni-catalyst for the hydrogenation of levulinic acid should be controlled for an optimization of the combined system. Zn can alone exert both functionalities although a high excess does not lead to a significant improvement in the GVL formation (Fig. S3†). On the other hand, the loading of nickel in the catalyst seem to be of paramount importance to reach high GVL production and low nickel loadings are required. Catalysts with low Ni-loading present small Ni nanoparticles whereas with high Ni-loading the size of nanoparticles is higher and, in some cases, these particles are not in contact with the support. In the catalyst with 2 wt% Ni the lower size of nanoparticles compared to the catalyst with 5 wt% leads to a higher amount of available active sites normalized per Ni loading in the catalyst with 2 wt%. However, only this factor cannot justify the higher activity normalized per Ni loading observed. Thus, it must be taken into account that the sepiolite free Ni catalyst presents very low activity per Ni loading. Therefore, the optimal Ni loading is 1–2 wt% and this is due not only to the higher amount of active sites per Ni loading but also likely to the higher reactivity of nanoparticles in close contact with the sepiolite.

The approach followed in the present article allows the use of remarkable low temperatures and the avoidance of the addition of pressurized H_2 because of the hydrogen generator role of Zn. It has been shown an example of the use of metals to react with water at very low temperature to generate H_2, this hydrogen being used for a subsequent transformation, and this strategy could be followed for some other reactions involving hydrogenation.

Materials and methods

Commercial Ni supplied by Alfa-Aesar-150–200 mesh was used for comparison. This sample was called as Ni.

Natural sepiolite was collected from Toledo (Castilla La Mancha, Spain) being supplied by Sepiolsa and was used as a support without previous treatment. The chemical analysis indicates that the support consists of 97.0% sepiolite, 1.9% dolomite and 1.1% other clays. Different Ni solutions were prepared by solving $Ni(NO_3)_2 \cdot 6H_2O$ (Sigma-Aldrich) in ethanol with oxalic acid ($H_2C_2O_4 \cdot 2H_2O$, Sigma-Aldrich), always being the molar Ni : oxalic ratio equal to 1 : 3. Sepiolite was added to the solution and evaporation of ethanol was carried out at 60 °C in a hotplate stirrer under vigorous stirring. These catalysts were labeled as *x*Ni/sep-ox, *x* being the Ni content (1, 2, 5 and 10 wt% were tested), and ox indicates that the catalysts were prepared by the impregnation method with oxalic acid.

For comparison, a simple 2 wt% Ni-loaded Ni/sepiolite catalyst obtained by wet impregnation was prepared similarly to Ni/sep-ox but in the absence of oxalic acid during the synthesis procedure. This catalyst was named as 2Ni/sep.

Finally, all samples were dried in a furnace at 100 °C for 6 h, and then heat-treated in static air for 2 h at 500 °C. Before reaction, catalysts were heat-treated in flowing H_2 for 2 h at 400 °C in order to reduce the metal oxide precursors.

Metallic Zn supplied by Alfa Aesar, CAS no.: 7440-66-6 has been used. To avoid oxidation, it has been kept under a nitrogen atmosphere and has been used in reaction as it is without subsequent transformation.

Characterization techniques

Catalysts were analyzed by high resolution transmission electron microscopy (HRTEM), using a field emission gun TECNAI G2 F20 microscope (FEI Company, Hillsboro, OR, USA), operated at 200 kV in order to analyze their structure and morphology. This equipment was also used for undertaking selected area electron diffraction (SAED) and energy dispersive X-ray spectroscopy (EDX). Catalysts samples for TEM were sonicated in absolute ethanol for 20 minutes and placed on a holey carbon film, which was supported on a copper grid. Finally, the copper grid was dried. TEM photographs were used to calculate the average size of the nickel particles. High resolution transmission electron microscopy (HRTEM) results were also obtained using a JEOL JEM 3000F (300 kV) microscope. Samples were prepared by crushing the powders under *n*-butanol and dispersing them over copper grids covered with a holey carbon film.

Powder X-ray diffraction (XRD) was employed in order to determine the crystalline phases of the samples. An Enraf Nonius FR590 sealed tube diffractometer (Bruker, Delft, The Netherlands) with a monochromatic Cu Kα_1 source operating at 40 kV and 30 mA was used.

Catalysts were submitted to N_2 adsorption at −196 °C, using a Micromeritics ASAP 2460 apparatus (Norcross, GA, USA). Catalysts were degassed at 150 °C before the analysis. Total pore volumes were determined, employing the adsorbed volume at a relative pressure of 0.99. A multipoint Brunauer–Emmet–Teller (BET) specific surface area (S_{BET}) was determined through the relative pressure range from 0.05 to 0.25. The pore size distribution was analyzed using the Barrett–Joyner–Halenda (BJH) method by analyzing the adsorption branch of the N_2 adsorption isotherms.

Catalytic tests and analyses

The catalytic conversion of LA into GVL was carried out using a 74 mL three neck flask. In standard experiments the flask was fed with 1.24 mmol of LA, 3.5 mL of water, 175.6 mg of catalysts and 171.6 mg of Zn.

The study of the influence of the Zn-loading was undertaken using 175.6 mg of catalyst and amounts of Zn varying from 0 to 285 mg. The flasks also contained 1.24 mmol of LA and 3.5 mL of water.

Another experiment was undertaken using two three neck flasks connected. One flask contained Zn (171.6 mg) and water (3.5 mL) and the other flask was filled with 1.24 mmol of LA, 3.5 mL of water and 175.6 mg of Ni-catalyst.

For all the experiments, the flasks were previously purged three times with N_2 in order to avoid the possible metal oxidation and later were sealed and introduced into a 30 °C water bath and stirred for 2 h. After that, the mixture was immediately filtered with the appropriate membrane to obtain the liquid phase containing the reaction product. Blanks in the absence of catalysts were carried out to check that GVL was not produced.

Analytical method

LA, GVL and the remaining reaction products were analyzed, as described in ref. 21 and 41.

The liquid samples were identified by gas chromatography, using the GC instrument Hewlett Packard 5890 (Palo Alto, California, USA), equipped with an Agilent HP-1 column (30 m × 0.32 mm × 0.25 μm). The detector employed was a FID detector working at 240 °C, and an injection port, working at 220 °C. The temperature program for a typical run was as follows: (i) 35 °C isothermal for 6 min, (ii) from 35 to 230 °C with a heating rate of 20 °C min^{-1}, and (iii) isothermal at 230 °C for 26 min. The retention times for GVL and LA were 5.4 and 9.5 min, respectively. Controls without LA and without catalysts were also analyzed to compare with the other reaction samples. Finally, liquid samples were also analyzed by gas chromatography mass spectrometer (GC-MS 5977A MSD-7890A, Agilent, Santa Clara, CA, USA) to identify other reaction byproducts. In this case, the retention times for GVL and LA were 12.4 and 16.4 min, respectively.

Gas analysis was undertaken to observe possible gas phase products and quantify the amount of hydrogen. This analysis was done utilizing a Hewlett Packard 5890 (Palo Alto, California, USA) gas chromatograph equipped with two columns: (i) Carbosieve-S and (ii) Porapak QS.

Conclusions

A novel green process has been envisaged for the hydrogenation of levulinic acid (LA) into γ-valerolactone (GVL) at very mild

conditions (30 °C, atmospheric pressure and LA water solution) using Ni-based catalysts supported on sepiolite without the external addition of hydrogen. Significantly, a redox reaction involving the oxidation of metallic Zn to ZnO for *in situ* hydrogen production throughout the water splitting reaction, instead of using high pressure molecular hydrogen, is proposed. Remarkable GVL yields up to 26% are obtained using an optimum Ni-supported catalyst prepared by impregnation with oxalic acid. For this catalyst, 80% of the nickel particles are smaller than 4 nm, which are homogeneously distributed on the external surface of the support. Accordingly, the presence of very small Ni nanoparticles finely dispersed on the sepiolite support seems to be the key parameter leading to remarkable productivities per Ni site. Regarding the role of Zn, *in situ* generated hydrogen demonstrates to be of paramount importance facilitating the hydrogenation of LA into GVL, since marginal GVL yield is achieved when gas phase hydrogen at atmospheric pressure is used in the reaction media.

Conflicts of interest

There are no conflicts to declare.

Acknowledgements

Authors from UCM thank MINECO (MAT2017-84118-C2-2-R project) and UCM CAI center of EM. Authors from UV thank MINECO (MAT2017-84118-C2-1-R project) and FEDER for funding. A. G. thanks MINECO for the pre-doctoral grant. SCSIE from UV is also acknowledged for characterization of the materials employed and the GC-MS analyses. Said Agouram is acknowledged for assistance in microscopy experiments. Miranda Sánchez is acknowledged for assistance in catalytic work.

References

1 T. D. Werpy, J. Holladay and J. F. White, *Top Value Added Chemical from Biomass: I. Results of Screening for Potential Candidates from Sugars and Synthesis Gas*, US Department of Energy, 2004, DOI: 10.2172/926125.
2 A. J. Ragauskas, C. K. Williams, B. H. Davison, G. Britovsek, J. Cairney, C. A. Eckert, W. J. Frederick Jr, J. P. Hallett, D. J. Leak, C. L. Liotta, J. R. Mielenz, R. Murphy, R. Templer and T. Tschaplinski, *Science*, 2006, **311**, 484–489.
3 D. Martin Alonso, S. H. Hakim, S. Zhou, W. Won, O. Hosseinaei, J. Tao, V. Garcia-Negron, A. H. Motagamwala, M. A. Mellmer, K. Huang, C. J. Houtman, N. Labbé, D. P. Harper, C. T. Maravelias, T. Runge and J. A. Dumesic, *Sci. Adv.*, 2017, **3**, 5.
4 H. Bhakta Sharma, A. K. Sarmah and B. Dubeya, *Renewable Sustainable Energy Rev.*, 2020, **123**, 109761.
5 R. C. Saxena, D. K. Adhikari and H. B. Goyal, *Renewable Sustainable Energy Rev.*, 2009, **13**, 167–178.
6 L. E. Manzer and K. W. Hutchenson, *US Pat.*, 6946563 B2, 2005.
7 L. Qi and I. T. Horváth, *ACS Catal.*, 2012, **2**, 2247–2249.
8 J. Cui, J. Tan, T. Deng, X. Cui, Y. Zhu and Y. Li, *Green Chem.*, 2016, **18**, 1619–1624.
9 J. Zhang, S. Wu, B. Li and H. Zhang, *ChemCatChem*, 2012, **4**, 1230–1237.
10 J. Q. Bond, D. M. Alonso, D. Wang, R. M. West and J. A. Dumesic, *Science*, 2010, **327**, 1110–1114.
11 S. Dutta, I. K. M. Yu, D. C. W Tsang, Y. H. Ng, Y. S. Ok, J. Sherwood and J. H. Clark, *Chem. Eng. J.*, 2019, **372**, 992–1006.
12 P. P. Upare, J. M. Lee, D. W. Hwang, S. B. Halligudi, Y. K. Hwang and J. S. Chang, *J. Ind. Eng. Chem.*, 2011, **17**, 287–289.
13 W. Luo, M. Sankar, A. M. Beale, Q. He, C. J. Kiely, P. C. A. Bruijnincx and B. M. Weckhuysen, *Nat. Commun.*, 2015, **6**, 6540–6550.
14 S. Cao, J. R. Monnier, C. T. Williams, W. Diao and J. R. Regalbuto, *J. Catal.*, 2015, **326**, 69–81.
15 W. Luo, U. Deka, A. M. Beale, E. R. H. van Eck, P. C. A. Bruijnincx and B. M. Weckhuysen, *J. Catal.*, 2013, **301**, 175–186.
16 S. Cao, J. R. Monnier and J. R. Regalbuto, *J. Catal.*, 2017, **347**, 72–78.
17 K. Shimizu, S. Kannoa and K. Kona, *Green Chem.*, 2014, **16**, 3899–3903.
18 S. Ishikawa, D. R. Jones, S. Iqbal, C. Reece, D. J. Morgan, D. J. Willock, P. J. Miedziak, J. K. Bartley, J. K. Edwards, T. Murayama, W. Ueda and G. J. Hutchings, *Green Chem.*, 2017, **19**, 225–236.
19 I. Orlowski, M. Douthwaite, S. Iqbal, J. S. Hayward, T. E. Davies, J. K. Bartley, P. J. Miedziak, J. Hirayama, D. J. Morgan, D. J. Willock and G. J. Hutchings, *J. Energy Chem.*, 2019, **36**, 15–24.
20 K. Sakakibara, K. Endo and T. Osawa, *Catal. Commun.*, 2019, **125**, 52–55.
21 R. Sanchis, T. García, A. Dejoz, I. Vázquez, F. Llopis and B. E. Solsona, *Materials*, 2019, **12**, 2918–2934.
22 K. Shimizu, S. Kanno and K. Kon, *Green Chem.*, 2014, **16**, 3899–3903.
23 K. Hengst, M. Schubert, H. W. P. Carvalho, C. Lu, W. Kleist and J. Grunwaldt, *Appl. Catal., A*, 2015, **502**, 18–26.
24 J. Lv, Z. Rong, Y. Wang, J. Xiu, Y. Wang and J. Qu, *RSC Adv.*, 2015, **5**, 72037–72045.
25 F. Jie, S. Dong and L. Xiuyang, *Catalysts*, 2016, **6**, 6–16.
26 S. Liu, M. Chen, L. Chu, Z. Yang, C. Zhu, J. Wang and M. Chen, *Int. J. Hydrogen Energy*, 2013, **38**, 3948–3955.
27 M. Ardakani, H. Mahabadi and A. Jafari, *J. Braz. Chem. Soc.*, 2019, **30**, 1933–1940.
28 C. Cerdá-Moreno, A. Chica, S. Keller, C. Rautenberg and U. Bentrup, *Appl. Catal., B*, 2020, **264**, 118546.
29 A. Alvarez, *Dev. Sedimentol.*, 1984, **37**, 253–287.
30 A. Guerrero-Torres, C. Jiménez-Gómez, J. Cecilia, C. García-Sancho, F. Franco, J. Quirante-Sánchez and P. Maireles-Torres, *Top. Catal.*, 2019, **62**, 535–550.
31 S. S. Enumula, V. R. B. Gurram, M. Kondeboina, D. R. Burri and S. R. R. Kamaraju, *RSC Adv.*, 2016, **6**, 20230–20239.
32 J. Yuan, S.-S. Li, L. Yu, Y. M. Liu, Y. Cao, H.-Y. He and K.-N. Fan, *Energy Environ. Sci.*, 2013, **6**, 3308–3313.

33 J. Feng, X. Gu, Y. Xue, Y. Han and X. Lu, *Sci. Total Environ.*, 2018, **633**, 426–432.
34 X. Du, L. He, S. Zhao, Y. Liu, Y. Cao, H. He and K. Fan, *Angew. Chem., Int. Ed.*, 2011, **50**, 7815–7819.
35 P. Son, S. Nishimura and K. Ebitani, *RSC Adv.*, 2014, **4**, 10525–10530.
36 P. P. Upare, M. Jeong, Y. K. Hwang, D. H. Kim, Y. D. Kim, D. W. Hwang, U. Lee and J. Chang, *Appl. Catal., A*, 2015, **491**, 127–135.
37 M. Chia and J. A. Dumesic, *Chem. Commun.*, 2011, **47**, 12233–12235.
38 K. Sakakibara, K. Endo and T. Osawa, *Catal. Commun.*, 2019, **125**, 52–55.
39 A. S. Amarasekara and M. A. Hasan, *Catal. Commun.*, 2015, **60**, 5–7.
40 I. Obregón, I. Gandarias, M. G. Al-Shaal, C. Mevissen, P. L. Arias and R. Palkovits, *ChemSusChem*, 2016, **9**, 2488–2495.
41 H. Zhong, Q. Li, J. Liu, G. Yao, J. Wang, X. Zeng, Z. Huo and F. Jin, *ACS Sustainable Chem. Eng.*, 2017, **5**, 6517–6523.
42 H. Gutbier and K. Hohne, *US Pat.* 3932600, January 13, 1976.
43 J. Petrovic and G. Thomas, *Reaction of Aluminum with Water to Produce Hydrogen*, U.S. Department of Energy, 2008.
44 A. Steinfeld, *Int. J. Hydrogen Energy*, 2002, **27**, 611–619.
45 C. Van Nguyen, B. Matsagar, J. Yeh, W. Chiang and K. Wu, *Mol. Catal.*, 2019, **475**, 110478.
46 J. Li, M. Li, C. Zhang, C. Liu, R. Yang and W. Dong, *J. Catal.*, 2020, **381**, 163–174.
47 D. Alonso-Domínguez, M. P. Pico, I. Álvarez-Serrano and M. L. López, *Nanomaterials*, 2018, **8**, 808–825.
48 Q. Tang, F. Wang, M. Tang, J. Liang and C. Ren, *J. Nanomater.*, 2012, 382603.
49 Z. Jiang, J. Xie, D. Jiang, X. Wei and M. Chen, *CrystEngComm*, 2013, **15**, 560–569.
50 A. M. Hengne, B. S. Kadu, N. S. Biradar, R. C. Chikate and C. V. Rode, *RSC Adv.*, 2016, **6**, 59753–59761.
51 B. Mallesham, P. Sudarsanam, B. Venkata Shiva Reddy, B. Govinda Rao and B. M. Reddy, *ACS Omega*, 2018, **3**, 16839–16849.